Near-infrared intersubband absorption in nonpolar cubic GaN/AlN superlattices

E. A. DeCuir, Jr., E. Fred, and M. O. Manasreh[a)]
Department of Electrical Engineering, University of Arkansas, Fayetteville, Arkansas 72701 and Department of Physics, University of Arkansas, Fayetteville, Arkansas 7270

J. Schörmann, D. J. As, and K. Lischka
Department of Physics, University of Paderborn, Paderborn 33095 Germany

(Received 19 June 2007; accepted 3 July 2007; published online 27 July 2007)

Optical absorption spectra related to intersubband transitions in molecular beam epitaxially grown nonpolar cubic-GaN/AlN superlattices were observed in the spectral range of 1.5–2.00 μm. The background doping was measured using an electrochemical capacitance-voltage technique and found to be on the order of 10^{18} cm^{-3}. This doping level yields a Fermi energy level slightly above the ground state energy level enabling intersubband transitions to occur. The existence of the intersubband transition is verified in several samples with different well widths. The observed peak position energy of the intersubband transition is compared to those calculated using a transfer matrix method. © *2007 American Institute of Physics*. [DOI: 10.1063/1.2764557]

In recent years, progress in hexagonal III-nitride epitaxial growth has extended the applications of this material system from the ultraviolet region to the near-infrared spectral region.[1–6] The ability to engineer quantum well structures consisting of $Al_{1-x}Ga_xN$ and GaN over a wide spectral range is made possible by the considerable conduction band offset between the two binaries AlN and GaN (~1.8 eV).[7] It is the magnitude of this band offset that theoretically enables the tuning of intersubband transition wavelengths towards the technologically important wavelengths such as 1.55 μm. Great strides in understanding the growth kinetics of hexagonal nitride materials have enabled steady progress in the growth and fabrication of detectors based on the intersubband transitions in GaN/AlN-based systems.[2–4,8,9] However, the large built-in electrostatic fields in polar hexagonal heterostructures grown on *c*-plane (0001) sapphire have been known to influence optical and electrical properties.[10,11] Efforts to circumvent these effects have been accomplished using *R*-plane $(10\bar{1}2)$ sapphire substrates which result in nonpolar *A*-plane $(11\bar{2}0)$ hexagonal nitride material, thus effectively eliminating the contributions of these large fields.[12,13]

In this letter, we report on the optical absorption due to the intersubband transition in nonpolar cubic GaN/AlN short period superlattices grown by plasma assisted molecular beam epitaxy on 3*C*-SiC substrates. To increase the optical absorption length, the samples were cut into waveguide geometry with the beveled facet having been polished at 45° to allow for multiple passes. The barrier and quantum well thicknesses of the structures were obtained from the reflection high energy electron diffraction (RHEED) intensity oscillations measured during the layer growth. The peak position energies of the room temperature optical absorption spectra of the intersubband transitions were observed in the spectral range of 1.5–2 μm. The peak position energies were calculated as a function of the well width by using a propagation matrix method. Good agreement was obtained between the calculated and measured values. A summary of the collected experimental data is contained in Table I.

All quantum structures were grown at 720 °C on freestanding 3*C*-SiC (001) substrates by plasma assisted molecular beam epitaxy. 100 nm thick *c*-GaN buffer was deposited on a 3*C*-SiC substrate using the RHEED control of the growth process as described in Ref. 14. Subsequently, a 20-period GaN/AlN superlattice (SL) was grown. The barrier thickness was fixed at 1.35 nm for all samples while the well thickness is changed for different samples, but kept in the range of 1.6–2.1 nm. Finally the quantum structures were capped with a 100 nm thick *c*-GaN layer. After each layer the growth was interrupted for 30 s to allow excess metal to evaporate from the surface. Three different superlattice samples with different quantum well widths were used in this study and waveguides were cut from each sample.

The optical absorption measurements were recorded using a Bruker Fourier-transform 125HR spectrometer. The interferometer configuration consists of a quartz-halogen light source, an InSb cooled detector, and a calcium fluoride beam splitter. This configuration permits the measurements in the spectral range of 1–3 μm. As mentioned above, the samples were cut into waveguide geometry to allow multiple passes of incident light through the active region. A transfer matrix method (also known as propagation matrix method) is used to calculate the bound state energy levels as a function of the well and barrier widths from which the energy difference between the ground and first excited states were obtained. These calculated values are then compared to the peak position energies obtained from the optical absorption spectra of the intersubband transitions.

The growth of the superlattice was controlled by RHEED. The intensity of the reflected electrons (RHEED intensity) was recorded at the start of the superlattice growth. Figure 1 shows the RHEED intensity versus time for the second and the third period as well as for periods 18 and 19. Since these measurements were continuous throughout growth, for clarity the time scans of periods 18 and 19 have been shifted both in time and in position to illustrate growth rate reproducibility. Since the spectra in this figure are

[a)]Electronic mail: manasreh@uark.edu

TABLE I. Summary of the 20-period cubic-GaN/AlN superlattice samples used in the present study. The period is obtained from the high resolution x-ray diffraction, L_W (nm) is the well width, E_{peak} is the peak position energy obtained from the experimental measurements, FWHM is the full width at half maximum of the intersubband transition spectra, n_{2D} is the two dimensional electron gas obtained by electrochemical capacitance measurements, and E_F is the Fermi energy level calculated from Eq. (1).

Sample number	Superlattice period (nm)	L_W (nm)	E_{peak} (meV)		FWHM (meV)	n_{2D} (10^{11} cm^{-2})	E_F (meV)
			Measured	Calculated			
A	3.45	2.1	620	630	182	2.79	3.52
B	3.1	1.75	696	734	211	2.33	2.94
C	2.95	1.6	751	781	219	2.13	2.68

shifted in time, the portions of the spectra represent that the interruption of the 30 s (areas between shaded portion of the figure) is shrunk The shaded areas indicate the growth of individual layers. All time scans are identical, which reveals a highly reproducible growth process of the quantum wells. Clear RHEED oscillations were observed during the nitrogen terminated growth of the AlN barrier layers revealing a growth rate of 0.11 ML/s. The cubic-GaN layers were grown with 1 ML coverage of Ga. The procedure to adjust the amount of excess Ga on the surface of the growing layer is described in detail in Ref. 14. Although the presence of the Ga adlayer prevents the observation of RHEED oscillations, i.e., *in situ* growth rate observation, the presence of this Ga adlayer is necessary for significant reduction of the GaN layer roughness. The growth rate of GaN was 0.26 ML/s, which is under nitrogen limited conditions.

The room temperature absorbance spectra of the intersubband transition in three superlattice samples are plotted in Fig. 2. Here we define the absorbance as the product of the absorption coefficient (α) and the total thickness of the quantum wells in the superlattice. In these coupled wells, splitting of the energy levels occurs due to overlap between localized wave functions in neighboring quantum wells, which leads to the formation of minibands. As summarized in Table I, the full width at half maximum (FWHM) of each absorption peak is relatively broad as compared to the FWHM of the intersubband transitions in other systems, such as GaAs/AlGaAs.[15] Notably the absorbance peak of sample C is close to the wavelength of 1.55 μm which is of relevance for the application of *c*-GaN/AlN SLs for optical communication light detectors.

A comparison between the experimental and calculated results of the peak position energy of the intersubband transition is shown in Fig. 3. The experimental data (represented by solid squares) were obtained directly from the peak position of the absorbance spectra while the calculated data (solid line) were obtained by taking the difference between the ground state (E_0) and the first excited state (E_1). The calculation was made for an electron effective mass of $0.19m_0$, where m_0 is the free-electron mass.[16] The experimental values are reasonably in good agreement with the calculated trend of the $E_0 \rightarrow E_1$ transition energy. An apparent improvement on this agreement can be obtained by increasing the effective mass. Again, the calculations are based on the transfer matrix approach.[17] The most important parameters which enter this calculation are the electron effective masses in the cubic-GaN well region and the ratio between the conduction and valence bands offsets (ΔE_{CV}). It was found that the best agreement between the experimental data and calculated results shown in Fig. 3 is when ΔE_{CV} =70:30. However, since ΔE_{CV} has not been thoroughly investigated for cubic III-nitrides, the ratio used here is similar to those reported for the hexagonal III-nitrides.[7]

In order for one to observe the intersubband transition in any quantum well system, the ground state needs to be populated with charge carriers. This can be achieved by doping the quantum well. In case of cubic GaN/AlN superlattices grown on cubic SiC, the background doping was found to be significantly high. In this study, the charge carrier concentra-

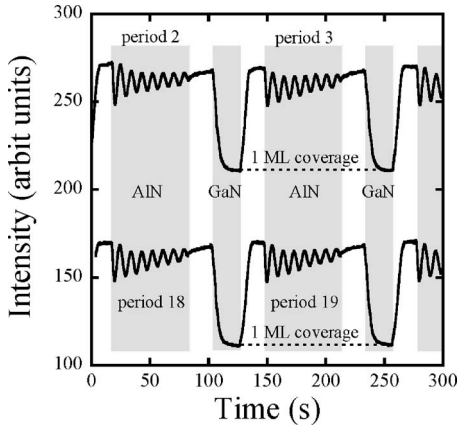

FIG. 1. RHEED intensity time scans measured during the growth of quantum wells number 2, 3, 18, and 19 of a 20-fold cubic GaN/AlN short period superlattice. The growth windows of the AlN and GaN layers are highlighted.

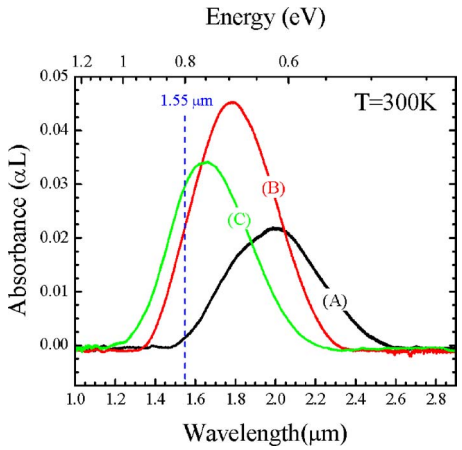

FIG. 2. (Color online) Room temperature absorbance spectra of three intersubband transitions measured for three cubic GaN/AlN superlattice samples with different well thicknesses.

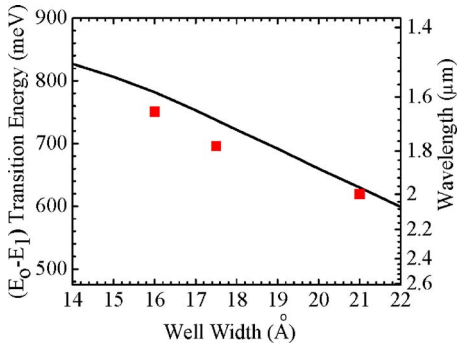

FIG. 3. (Color online) Peak position energies of the intersubband transitions in cubic GaN/AlN superlattices measured (solid squares) and calculated (solid line) as a function of GaN well width.

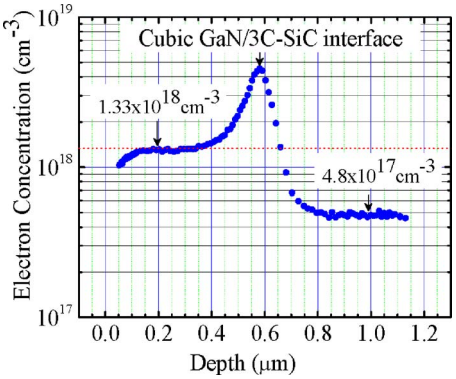

FIG. 4. (Color online) Charge carrier concentration in a reference thick cubic GaN layer measured as a function of etch depth using an electrochemical capacitance-voltage profiler.

tion was measured using an electrochemical capacitance-voltage profiler (ECVPro). Since etching AlN is very difficult due to the fact that the ultraviolet light used in the ECVPro system does not cover the band gap of AlN, a reference sample with thick cubic GaN layer was grown under the same growth conditions as those of the GaN/AlN superlattices. This reference layer was tested using the ECVPro system and the results are shown in Fig. 4. It is clear from this figure that the bulk carrier concentration (N_{3D}) as a function of the etched depth is on the order of 1.33×10^{18} cm^{-3}. The peak observed at the depth of 0.6 μm in the carrier concentration is due the charge accumulation at the GaN/SiC interface.

By using the well widths determined from RHEED oscillation, confirmed by the high resolution x-ray diffraction measurements, and the measured three-dimensional carrier concentration of unintentionally doped cubic GaN, the Fermi energy level (E_F) position in the superlattices is calculated using the following expression:[18]

$$E_F \approx E_0 + n_{2D}\pi\hbar^2/m^*, \quad (1)$$

where n_{2D} is the two-dimensional electron concentration, $\hbar$ is the Planck constant, and m^* is the effective mass. The calculated values of E_F are listed in Table I for three samples. Since the well width is small and the effective mass is relatively large, the calculated Fermi energy level is slightly above the ground state. Nonetheless, this condition is sufficient for population of the ground state with electrons, which is a necessary condition to observe of intersubband transitions.

In conclusion, intersubband transitions are observed in the near-infrared spectral region in cubic-GaN/AlN short period superlattices grown on cubic SiC substrates. Growth refinement of cubic nitride has enabled the observation of intersubband transitions in this system in the absence of piezoelectric effect. The electrochemical capacitance-voltage measurements confirm the presence of relatively high carrier concentrations in the cubic GaN system investigated here. Good agreement between the experimentally measured and calculated peak position energies of the intersubband transition is obtained. The calculated peak position energies were obtained using a transfer matrix model. The optical absorption measurements confirm the tuning of the intersubband transition in cubic GaN/AlN to the near-infrared spectral region. In particular, the peak position of the intersubband transition spectrum reached the 1.55 μm spectral region, which is an important region for optical communications.

The work at the University of Arkansas was funded by the Air Force Office of Scientific Research (program manager: Gernot Pomrenke) and by the Arkansas Science & Technology Authority. The authors would like to thank H. Nagasawa and M. Abe from SiC Development Center, HOYA Corporation, Japan, for supplying the 3*C*-SiC substrates.

[1] E. A. DeCuir, E. Fred, B. S. Passmore, A. Muddasani, M. O. Manasreh, J. Xie, H. Morkoc, M. E. Ware, and G. J. Salamo, Appl. Phys. Lett. **89**, 1 (2006).
[2] D. Hofstetter, E. Baumann, F. R. Giorgetta, M. Graf, M. Maier, F. Guillot, E. Bellet-Amalric, and E. Monroy, Appl. Phys. Lett. **88**, 121112 (2006).
[3] F. Guillot, E. Bellet-Amalric, E. Monroy, M. Tchernycheva, L. Nevou, L. Doyennette, F. H. Julien, L. S. Dang, T. Remmele, M. Albrecht, T. Shibata, and M. Tanaka, J. Appl. Phys. **100**, 044326 (2006).
[4] E. Baumann, F. R. Giorgetta, D. Hofstetter, H. Lu, X. Chen, W. J. Schaff, L. F. Eastman, S. Golka, W. Schrenk, and G. Strasser, Appl. Phys. Lett. **87**, 191102 (2005).
[5] B. K. Ridley, W. J. Schaff, and L. F. Eastman, J. Appl. Phys. **94**, 3972 (2003).
[6] N. Suzuki, N. Iizuka, and K. Kaneko, Jpn. J. Appl. Phys., Part 1 **42**, 132 (2003).
[7] I. Vurgaftman, J. R. Meyer, and L. R. Ram-Mohan, J. Appl. Phys. **89**, 5815 (2001).
[8] Hadis Morkoc, *Nitride Semiconductors and Devices Springer Series in Materials Science* (Springer, Berlin, 1999), Vol. 132, p. 488.
[9] T. G. Andersson, X. Y. Liu, T. Aggerstam, P. Janes, P. Holmstrom, S. Lourdudoss, and L. Thylen, J. Cryst. Growth **301-302**, 457 (2007).
[10] O. Ambacher, R. Dimitrov, M. Stutzmann, B. E. Foutz, M. J. Murphy, J. A. Smart, J. R. Shealy, N. G. Weimann, K. Chu, M. Chumbes, B. Green, A. J. Sierakowski, W. J. Schaff, and L. F. Eastman, Phys. Status Solidi B **216**, 381 (1999).
[11] Seoung-Hwan Park and Shun-Lien Chuang, Appl. Phys. Lett. **76**, 1981 (2000).
[12] C. Gmachl and H. M. Ng, Electron. Lett. **39**, 567 (2003).
[13] E. Kuokstis, W. H. Sun, C. Q. Chen, J. W. Yang, and M. A. Khan, J. Appl. Phys. **97**, 103719 (2005).
[14] J. Schörmann, S. Potthast, D. J. As, and K. Lischka, Appl. Phys. Lett. **90**, 041918 (2007).
[15] K. K. Choi, B. F. Levine, R. J. Malik, J. Walker, and C. G. Bethea, Phys. Rev. B **35**, 4172 (1987).
[16] K. Kim, W. R. L. Lambrecht, B. Segall, and M. Van Schilfgaarde, Phys. Rev. B **56**, 7363 (1997).
[17] Paul Carter Harrison, *Quantum Wells, Wires and Dots: Theoretical and Computational Physics of Semiconductor Nanostructures* (Wiley, New York, 2005), p. 17.
[18] M. O. Manasreh, *Semiconductor Heterojunctions and Nanostructures* (McGraw-Hill, New York, 2005), p. 174.